Setting up roadblocks for kinesin-1: mechanism for the selective speed control of cargo carrying microtubules†

Till Korten and Stefan Diez*

Received 3rd March 2008, Accepted 3rd July 2008
First published as an Advance Article on the web 30th July 2008
DOI: 10.1039/b803585g

Motor-driven cytoskeletal filaments are versatile transport platforms for nanosized cargo in molecular sorting and nano-assembly devices. However, because cargo and motors share the filament lattice as a common substrate for their activity, it is important to understand the influence of cargo-loading on transport properties. By performing single-molecule stepping assays on biotinylated microtubules we found that individual kinesin-1 motors frequently stopped upon encounters with attached streptavidin molecules. Consequently, we attribute the deceleration of cargo-laden microtubules in gliding assays to an obstruction of kinesin-1 paths on the microtubule lattice rather than to 'frictional' cargo-surface interactions. We propose to apply this obstacle-caused slow-down of gliding microtubules in a novel molecular detection scheme: Using a mixture of two distinct microtubule populations that each bind a different kind of protein, the presence of these proteins can be detected *via* speed changes in the respective microtubule populations.

Introduction

Biomolecular motors are promising components for the setup of molecular sorting and nano-assembly devices.[1–4] In particular, *in vitro* transport assays often utilize the geometry of gliding motility where motor proteins are adsorbed onto a substrate surface and propel cytoskeletal filaments in the presence of ATP.[5–7] Nano-sized cargo is then most commonly attached to these filaments *via* biotin and streptavidin.[8–14] While motile filaments provide a versatile platform for attachment of transport material, heavy cargo-loading was reported to significantly decelerate gliding motion.[10] However, the details of this effect have remained unclear.

Max Planck Institute of Molecular Cell Biology and Genetics, Pfotenhauerstraße 108, D-01307, Dresden, Germany. E-mail: diez@mpi-cbg.de; Fax: +49-351-210-2020; Tel: +49-351-210-2521

† Electronic supplementary information (ESI) available: See DOI: 10.1039/b803585g

‡ Movie S1. Single-molecule stepping assays on streptavidin-coated microtubules. Typical movies of single kinesin molecules walking on microtubules (after streptavidin incubation) with the biotinylation ratios indicated above each microtubule. Microtubule positions were derived from a single image taken before the kinesin stream and are shown in red. Green signals represent GFP–kinesin. The movie plays with 3× real-time speed in order to better distinguish moving from stopping kinesins.

§ Movie S2. Dual color stream of a typical encounter between a GFP–kinesin molecule and a Qdot roadblock. The GFP channel is shown in green, the Qdot 655 channel in red. GFP and Qdot channels were separated by a beam splitter, imaged simultaneously on separate halves of the camera chip and overlaid with the help of multi-color fluorescent tetraspeck beads. The arrow indicates the GFP–kinesin molecule that walks along the microtubule, stops at the position of the Qdot, continues walking and detaches. The movie was slowed down 3× relative to real-time.

¶ Movie S3. Selective slow-down of biotinylated fluorescein labeled (green) or rhodamine labeled (red) microtubule populations incubated with combinations of non-fluorescent streptavidin (SA) and rhodamine antibodies (AB) in the same gliding assay. Time-lapse fluorescence movies of both fluorescence channels upon the addition of SA and/or AB as indicated below each panel. The movie plays with 10× real-time speed.

To investigate this phenomenon, we performed systematic gliding and stepping motility experiments (see Fig. 1). As the transport system we used kinesin-1 (henceforth denoted "kinesin") motors and biotinylated microtubules loaded with varying amounts of streptavidin (our model cargo). By monitoring microtubule speed in gliding assays, we characterized slow-down as a function of streptavidin concentration on the microtubule lattice. In complementary single molecule stepping experiments we investigated the mechanism behind this cargo-induced deceleration.

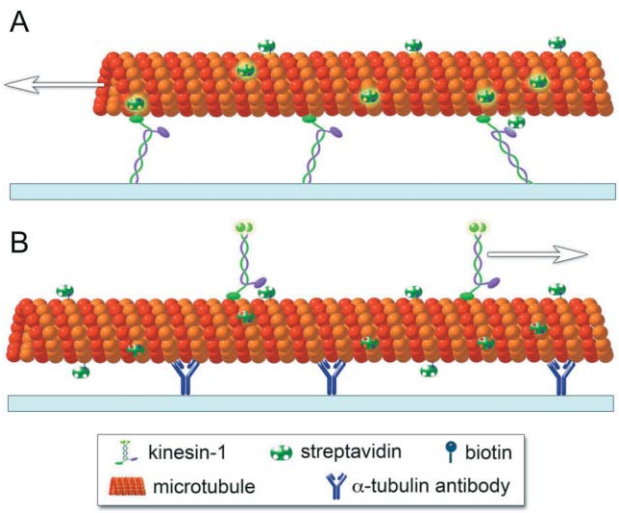

Fig. 1 Schematics of the utilized *in vitro* motility assays. (A) Gliding assay where streptavidin-coated microtubules glide over a surface coated with kinesin motors. (B) Stepping assay where GFP–labeled kinesin molecules move along streptavidin-coated microtubules that are fixed to the surface *via* tubulin antibodies.

Beyond an improved understanding of the interaction between kinesin and cargo-laden microtubules, we propose that microtubule slow-down can, in return, be utilized for a novel

molecular detection scheme. Because cargo density on the microtubule lattice translates into a predictable change of gliding speed it is possible to infer the concentration of such cargo from speed measurements. To demonstrate this principle, we simultaneously detected the presence of rhodamine antibodies and streptavidin in our motility solution by using a mixture of regular microtubules labeled with rhodamine and biotinylated microtubules labeled with fluorescein.

Materials and methods

Experiments were performed in 1.5 to 2 mm-wide flow cells self-built from two glass coverslips (Corning, 22 × 22 mm^2 and 18 × 18 mm^2) glued together by heated pieces of Nescofilm (Roth, thickness 0.1 mm).

Microtubule preparation

Microtubules were polymerized from 5 μl of bovine brain tubulin (4 mg ml^{-1}, Cytoskeleton Inc.) in BRB80 buffer (80 mM potassium PIPES, pH 6.9, 1 mM EGTA, 1 mM $MgCl_2$, if not specifically mentioned, all chemicals were purchased from Sigma) with 4 mM $MgCl_2$, 1 mM Mg-GTP, and 5% DMSO at 37 °C. After 60 min, the microtubule polymers were stabilized and diluted 100-fold in BRB80 containing 10 μM taxol at room temperature. Fluorescently labeled and biotinylated microtubules were created by mixing labeled tubulin (rhodamine and fluorescein) with biotinylated and non-labeled tubulin before microtubule assembly.

Gliding assays

For gliding assays, a casein-containing solution (0.5 mg ml^{-1} in BRB80 (80 mM PIPES)/KOH pH 6.9, 1 mM EGTA, 1 mM $MgCl_2$) was perfused into a flow cell and allowed to adsorb to the surfaces for 5 min. Next, 50 μl of a motor solution containing 2 μg ml^{-1} wild-type kinesin in BRB80 (full length drosophila conventional kinesin expressed in bacteria and purified as previously described[15]) was perfused into the flow cell and allowed to adsorb for 5 min. Thereafter, a motility solution (1 mM ATP, 20 mM D-glucose, 20 μg ml^{-1} glucose oxidase, 10 μg ml^{-1} catalase, 0.5% 2-mercapto-ethanol, 10 μM taxol in BRB80) containing fluorescently labeled taxol-stabilized microtubules was applied. Speed measurements were performed directly before streptavidin treatment and after the final washing step.

Stepping assays

In stepping assays we used flow channels (see above) made of glass coverslips which were cleaned in piranha solution (H_2O_2/H_2SO_4, 3 : 5; **Caution:** corrosive, gets hot during mixing) before silanization with 0.05% dichlorodimethylsilane in trichloroethylene. To immobilize microtubules, channels were incubated with 0.5 μM monoclonal anti-β-tubulin antibody produced in mouse clone TUB 2.1 in BRB80 for 5 min, followed by 30–60 min with 1% Pluronic F-127 in BRB80, and finally microtubules in BRB80 for 5 min. Channels were rinsed with BRB20 (20 mM PIPES-/KOH pH 6.9, 1 mM $MgCl_2$, 1 mM EGTA) before addition of the imaging solution (BRB20 supplemented with 0.1 mg ml^{-1} casein, 1 mM ATP, 2% 2-mercaptoethanol, 40 mM glucose, 40 μg ml^{-1} glucose oxidase, 20 mg ml^{-1} catalase, and 2.5 nM truncated, GFP–labeled kinesin-1 constructs (rkin430GFP), which contained the first 430 amino acids of kinesin-1 fused to a GFP and a polyhistidine tag at the tail domain, cloning and purification have been described[16]). Single molecule recordings were performed before and after streptavidin treatment.

BRB20 (a low salt buffer) was used for stepping experiments because in this buffer a 10 times lower kinesin concentration was sufficient to generate the same number of events as in BRB80. This significantly reduced the background caused by non-specific binding of kinesin to the surface. However, the ratio of moving to non-moving kinesin was comparable when we used BRB80 (tested for non-biotinylated and 1 : 4 biotinylated microtubules).

Streptavidin coating of microtubules

Streptavidin coating of gliding and surface-immobilized microtubules was performed by washing out unbound microtubules and flowing a streptavidin solution (10 μM streptavidin (Pierce) or 10 μM fluorescein-labeled streptavidin (Pierce) in motility solution, unless stated differently) into the flow cell. Streptavidin was removed after 10 min of incubation by washing twice with motility solution. The same procedure was applied for streptavidin and rhodamine antibody coating in the molecular detection experiment.

Detection of antibody binding to streptavidin-coated microtubules

Streptavidin-coated microtubules were prepared as described above. Flowchannels were then perfused with a solution of 100 nM fluorescein isothiocyanate (FITC) conjugated polyclonal anti-streptavidin antibody produced in rabbit (Rockland Immunochemicals) and 1 μM biotin (to block a biotin cross-reactivity of the antibody) in motility solution. After 10 min this solution was washed out twice with motility solution and the microtubule speeds were measured after 5 min temperature equilibration.

Image acquisition and data analysis

Fluorescence images were obtained using two microscope setups, both based on a Zeiss Axiovert 200 M inverted optical microscope: (i) Gliding assays were observed by epi-fluorescence using a 40× air objective (NA 0.75) or a 100× oil immersion objective (NA 1.3) and filter sets for the rhodamine (excitation (exc) 535/50, dichroic (dc) 565 longpass (LP), emission (em) 610/75) and the fluorescein channel (exc 480/40, dc 505 LP, em 535/50). Images were acquired with an exposure time of 100 ms in timelapse mode (one frame every 1 s for single color and one frame every 3.5 s for dual color recordings) by a back-illuminated CCD camera (MicroMax 512 BFT, Roper Scientific) in conjunction with a Metamorph imaging system (Universal Imaging Corp.) Microtubule speeds were measured manually, tracing the microtubule paths over a period of 20 s in the acquired timelapse movies. The fluorescence intensity per micrometer of fluorescein–streptavidin-coated microtubule was measured by summing up the intensity counts of the brightest pixels in a 6 pixel wide line-scan along the microtubule axis, subtracting

the average background and dividing by the microtubule length in micrometers. Each value represents the mean ± s.d. of 8–13 microtubules. (ii) Stepping assays were observed by total internal reflection fluorescence (TIRF) microscopy using a 100× oil immersion objective (Zeiss APOCHROMAT NA 1.46) and a mixed gas argon–krypton laser (Innova 70C Spectra; Coherent). Image acquisition was performed with 100 ms exposure in streaming mode by an electron-multiplied CCD camera (iXon DV 897, Andor) in conjunction with a Metamorph imaging system (Universal Imaging Corp., Downington, PA). In the evaluation of the moving and stopping dwell times (Fig. 3), only events where the motors landed during acquisition were counted to avoid errors from the accumulation of dead motors. Single particle tracking was performed using an in-house software based on MatLab (Mathworks, Natick, MA). The algorithm uses two-dimensional Gaussian fitting (least squares method; variable width of Gaussian) of the pixelated intensity profiles arising from single particles.

For simultaneous dual color recordings a spectral beam splitter (W-view A8509, Hamamatsu) was used. The signals of the two color channels were recorded on two different halves of the same CCD camera chip. To align the dual-color images with respect to each other—and as a drift control for tracking—multifluorescent TetraSpeck beads (0.2 µm diameter, Mo Bi Tec) were diluted 200-fold in BRB80 and additionally perfused into the flow chambers (incubation time 5 min) before the flow sequence of the stepping assays described above. The following filters (Chroma Technology, if not stated otherwise) were used for imaging: exc 488/10, em 660/50, dc 505 LP for 488 nm laser excitation with single-color detection and exc 475/42 (Semrock), em dual-band 527–645 (Semrock), dc 488LP (Semrock) for arc-lamp excitation with dual-color detection. The W-view beamsplitter was equipped with: em 660/40, em 531/40 (Semrock), dc 590dcxr, and dc Q590dcspxr.

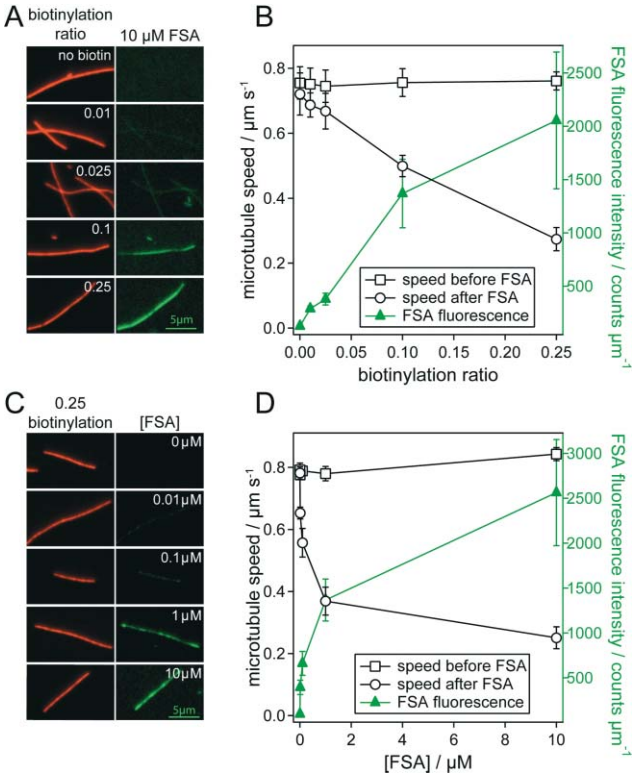

Fig. 2 Dependence of microtubule speed on FSA coating density. (A), (C) Fluorescence images of FSA-coated, rhodamine-labeled microtubules in the rhodamine (red) and fluorescein (green) channels. (B), (D) Gliding speeds of microtubules before (black, open squares) and after (black, open circles) FSA incubation (mean ± s.d., $n = 20$). Corresponding FSA fluorescence intensities are shown as green, filled triangles (right axes, mean ± s.d, $n = 6$). In (A) and (B) microtubules with various biotinylation ratios were incubated with 10 µM FSA. In (C) and (D) microtubules with a fixed biotinylation ratio of 1 : 4 were incubated with varying concentrations of FSA.

Results and discussion

Microtubule gliding speed depends on the streptavidin coating density

We first studied the impact of cargo loading on the gliding speed of rhodamine-labeled, biotinylated microtubules that were loaded with varying amounts of fluorescein-labeled streptavidin (FSA, see Fig. 1A). We changed the streptavidin density on the microtubule lattice either (i) by varying the microtubule biotinylation ratio and adding a fixed (saturating) amount of FSA (Fig. 2A and B) or (ii) by using a fixed biotinylation ratio and varying the FSA concentration (Fig. 2C and D). For all FSA concentrations used in this second experiment, FSA was in excess compared to the estimated amount (100 pM) of biotin binding sites on the microtubules. However, the biotin binding sites were only saturated within the given incubation time at 10 µM FSA as observed by the clustering of motile microtubules at lower FSA concentrations. This is indicative of a varying FSA density on the microtubules. Images were acquired by fluorescence microscopy in the rhodamine and in the fluorescein channel (Fig. 2A and C). (Fig. 2B and D show the gliding speeds before (open squares) and after (open circles) FSA treatment. The actual FSA coating density was estimated from the green fluorescence intensity of the coated microtubules (green, filled triangles). Before incubation with FSA, no significant dependence of microtubule speed on biotinylation ratio was observed. On the other hand, after FSA incubation, a significant decrease in microtubule speeds with increasing FSA 'decoration' occurred. This shows that small molecules like rhodamine or biotin do not impact microtubule gliding. However, molecules like streptavidin—that are in the size-range of motor heads—are able to hinder microtubule movement. The linear dependence of microtubule speed on FSA coating density was confirmed by plotting microtubule speeds (data from Fig. 2B and D, open circles) against the corresponding FSA fluorescence intensities (data from Fig. 2B and D, green filled triangles). This plot could be fitted well by a linear function (Pearson's $r = -0.944$).

Single kinesin molecules stop on streptavidin coated microtubules

To test whether the observed deceleration of microtubules originated from direct kinesin–streptavidin interactions, we studied the behavior of individual kinesin motors on microtubules coated with non-fluorescent streptavidin in stepping assays. Trajectories of GFP-labeled motors were recorded by total-internal reflection fluorescence (TIRF) microscopy (ESI movie S1‡) and evaluated in space-time plots ('kymographs').

Fig. 3A shows typical kymographs of individual GFP–kinesin molecules stepping on biotinylated and streptavidin-coated microtubules. While control measurements on non-biotinylated microtubules (or biotinylated microtubules without streptavidin treatment) showed trajectories characteristic for kinesin (speed of about $0.54 \pm 0.14\,\mu m\,s^{-1}$, typical for the low salt concentration (BRB20) used in our assay), a less robust motility was identified for increasing streptavidin decoration. In order to perform a quantitative analysis of this behavior, we classified the different motility events in the following manner (Fig. 3B): a 'moving kinesin' translated with constant speed, a 'non-moving kinesin' did not change its position, a 'stopping kinesin' switched from the moving to the non-moving state, a 'starting kinesin' switched from the non-moving to the moving state and a 'pausing kinesin' stopped first and started again later.

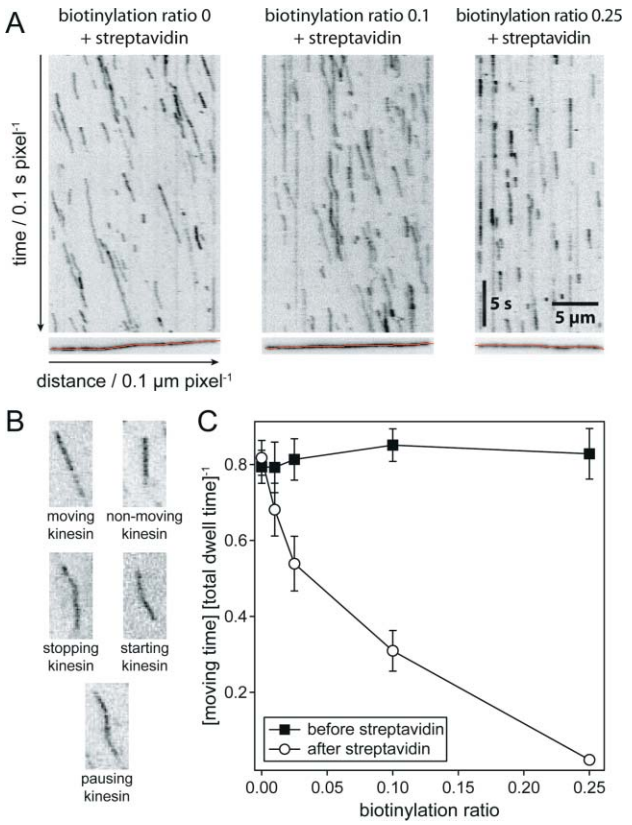

Fig. 3 Single-molecule stepping assays on streptavidin-coated microtubules. (A) Typical kymographs of single kinesin molecules walking on microtubules with different biotinylation ratios (after streptavidin incubation). Time is progressing from top to bottom, while the motors (dark signals) move along a surface-immobilized microtubule from left to right. Small images below each kymograph show how its space dimension was derived from a line drawn across the corresponding microtubule. (B) Classification of the different motility events. (C) Ratio of integrated moving time to total dwell time (moving time + non-moving time) of all kinesin binding events (usually around 80) per microtubule. Each data point represents an average over 6 microtubules, weighted by the total dwell time. Error bars represent unbiased estimators for the population standard deviation ($n = 6$).

Based on this classification, we then plotted the ratio of integrated moving times to total dwell times as a function of the microtubule biotinylation ratio (Fig. 3C). Before incubation with streptavidin, no significant dependence on biotinylation ratio was observed. In contrast, after microtubules were incubated with streptavidin, the number of non-moving and stopping kinesin molecules significantly increased. Hence the relative time kinesin molecules spent in moving phases (and such the plotted ratio) decreased with increasing streptavidin coating density. However, in-between stopping events the motors always moved at full speed, independent of microtubule biotinylation ratio and streptavidin incubation.

While the stopping we observe here agrees with other single molecule experiments performed under steady state conditions (*i.e.* during processive movement of motors in the presence of ATP),[17] it might conflict with previous light scattering experiments.[18] In these experiments, wild-type kinesin was bound in rigor state at high densities (up to one kinesin molecule per tubulin dimer) to microtubules in the presence of static roadblocks. Upon addition of ATP and subsequent relaxation into steady-state, kinesin appeared to release very rapidly. However, in ref. 18 this release was related to the relaxation process from rigor state to steady state.[19]

Observing kinesin stopping at roadblocks with nanometer resolution

To test if the stopping positions of individual GFP–kinesin molecules correlated with the locations of obstacles, we performed stepping experiments with streptavidin-coated quantum dots (Qdots, emission wavelength 655 nm) attached to the microtubule lattice. Using a dual-color emission beam-splitter, we tracked Qdots and GFP–kinesin molecules simultaneously with a tracking software developed in our lab.[20] The tracking accuracy for individual Qdots and GFP–kinesin molecules was estimated to be 7 nm and 30 nm, respectively.

A typical example of an encounter between a GFP–kinesin molecule and a Qdot is provided in Fig. 4 and ESI movie S2.§ The x–y trajectories (Fig. 4A) clearly show that the GFP–kinesin molecule (green trace) walked in a straight line until it encountered a Qdot (red trace). The motor then stopped for a while and continued walking eventually. For a better illustration of the temporal component, the distance of both trajectories from the average Qdot position was plotted against time in a kymograph-like manner (Fig. 4B). To calculate the distance along the microtubule, all tracked positions were projected onto the direction of the microtubule, derived from a linear regression of the GFP–kinesins x–y data.

From our data on the stepping of GFP–kinesin, we conclude that streptavidin molecules or Qdots form immobile 'roadblocks' which stop kinesin motors without causing them to detach. This can be explained by kinesin's particular properties: Kinesin moves in a hand-over-hand mechanism along a single protofilament.[21–23] Its processivity requires the rear head to stay bound until the leading head is firmly attached to the next tubulin dimer along the protofilament.[24,25] Therefore, if a large molecule is blocking the next tubulin dimer, the leading head cannot bind and the rear head cannot detach. This situation effectively stalls the kinesin molecule. In a gliding assay, where each microtubule is transported by many kinesin motors, the stalling of some kinesin molecules causes a significantly increased drag force during the period of their attachment and provides an

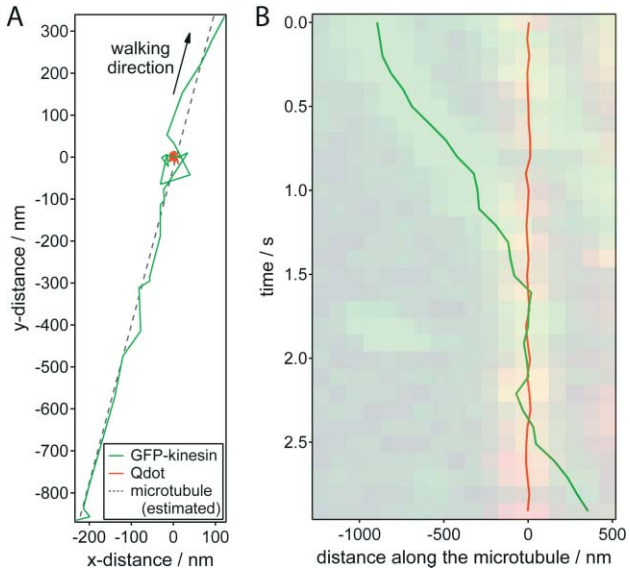

Fig. 4 Nanometer tracking of a typical encounter between a GFP–kinesin molecule and a Qdot roadblock. (A) *x*–*y* trajectories of the GFP–kinesin molecule (green) and Qdot (red). The microtubule position was estimated by linear regression of the GFP–kinesin data (dotted line). (B) Distance of the GFP–kinesin molecule and the Qdot along the microtubule (relative to the average position of the Qdot) plotted against time. The dual color kymograph, derived from the widefield TIRF imaging was put transparently in the background for comparison.

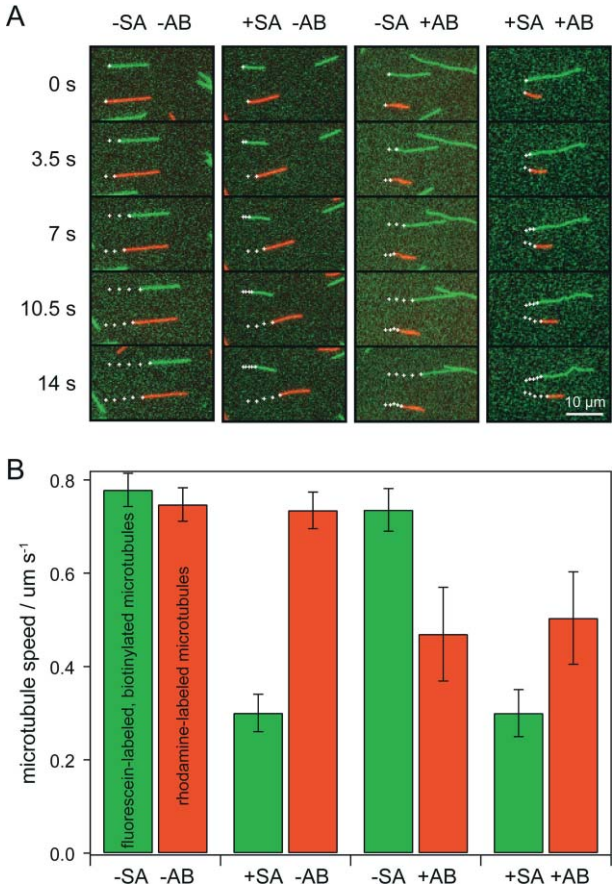

Fig. 5 Selective slow-down of biotinylated fluorescein labeled (green) or rhodamine labeled (red) microtubule populations incubated with combinations of non-fluorescent streptavidin (SA) and rhodamine antibodies (AB) in the same gliding assay. (A) Time-lapse fluorescence images of both fluorescence channels upon the addition of SA and/or AB. The paths travelled by the microtubules in a given time period are indicated by white crosses. (B) Average speeds of the individual microtubule population. Error bars represent the standard deviation for 20 microtubules.

explanation for the slow-down of gliding microtubules (see also Fig. 1A for a schematic drawing). This is also supported by the fact that we observed occasional stopping and jerky movement of short microtubules in gliding assays with low kinesin density (data not shown). However, usually we used high kinesin densities and therefore the speeds measured for Figs. 2 and 5 were uniform, *i.e.* did not represent the averages of fast movement and pauses. We therefore believe, that the observed deceleration of cargo-laden microtubules in gliding assays is caused by an obstruction of kinesin pathways on the microtubule lattice rather than by 'frictional' cargo–surface interactions.

Interestingly, about half of the stopped kinesin molecules were able to overcome the obstacles eventually (representative events shown by the pausing kinesins in Fig. 3C and Fig. 4). One way to explain this behavior is that kinesin molecules are able to pass obstacles during their processive runs. This would be possible if obstacles and kinesin molecules do not occupy the same binding sites on the polymerized tubulin dimers. Molecular flexibility could then allow motors to pass obstacles—their stepping probability still being sufficiently reduced to account for the observed non-moving phases. Alternatively, the motors could temporarily detach from the microtubule, diffuse two-dimensionally along the microtubule lattice and rebind adjacent to—or past—the obstacle. A similar diffusion has recently been identified for kinesin-13 and kinesin-5,[26,27] two other members of the kinesin superfamily. Kinesin's ability to overcome obstacles agrees with its operation on highly crowded microtubules *in vivo*. The obstacles which kinesin encounters *in vivo* have probably been adapted by evolution to complement the functions of the motor protein. The impact of microtubule decoration on kinesin activity most likely strongly depends on whether a microtubule-associated protein occupies a different[28] or the same[17] binding site as kinesin. Recently, Tau, which is abundant in neurons, has been reported to cause kinesin to detach from microtubules.[29] This behavior, which is distinctly different from the behavior reported here, has been hypothesized to be a specific biological function of Tau involved in the targeting of cargo transported by kinesin.

Simultaneous detection of two different protein species

Based on the observation that the gliding speed of decorated microtubules decreases in a linear manner with loading density we propose to employ microtubule speed measurements for the detection of molecular compounds present in a given test sample (Fig. 5). To demonstrate this principle, we used two distinct microtubule populations in one gliding assay: fluorescein labeled microtubules (shown in green) with a biotinylation ratio of 0.25 and non-biotinylated rhodamine labeled microtubules (shown in red). This microtubule mixture was then incubated with 10 µM non-fluorescent streptavidin and/or 10 nM non-fluorescent rhodamine antibodies.

Time-lapse fluorescence images of typical microtubules of each population are shown in Fig. 5A and ESI movie S3¶ together with the corresponding speed measurements in Fig. 5B. Before incubation with streptavidin or rhodamine antibodies, both populations moved with similar speeds. After incubation with streptavidin, green microtubules slowed down to about 40% of their original speed while the speed of red microtubules remained unaffected. Similarly, incubation with rhodamine antibodies slowed down red microtubules to about 60% of their original speed without affecting green microtubules. After incubation with both reagents at the same time, both microtubule populations were slowed down.

These results show that a novel, highly-sensitive mechanism for molecular detection becomes possible when several microtubule populations (that specifically bind the molecules or particles of interest) are used. Measuring their speeds after incubation with a test sample and relating the obtained values to an inert control population would then allow a quantitative inference about the molecular composition of the test solution. For distinguishable fluorescence detection different microtubule populations might be labeled with a number of different fluorophores. Upscaling to a high number of different microtubule populations can be achieved by patterns of different fluorophores in a bar-code like fashion.[30] Versatile linkers to the molecules of interest can be provided by the antigen binding fragments of antibodies (Fab fragments) or aptamers[31] that are chemically crosslinked to the lattices of microtubules. This flexibility provides a crucial advantage of our proposed method over earlier reports where the gliding speed of actin filaments was used for the detection of mercuric ions.[32] There, the slow-down mechanism was based on the covalent reaction of mercuric ions with the motor proteins themselves.

Detecting the binding of an analyte to streptavidin

In order to detect a wide variety of analytes the use of analyte-specific Fab fragments or aptamers linked to the microtubule lattice is necessary. However, because Fab fragments are comparable in size to streptavidin (~50 kDa), one might expect them to act as roadblocks themselves. Even aptamers (~10 kDa)—while much smaller than Fab fragments—are still a lot larger than the rhodamine or biotin modifications which we tested to have no effect on microtubule speed. We therefore investigated if the binding of FITC-conjugated, polyclonal anti-streptavidin antibody (anti-SA-AB, the 'analyte') to streptavidin-coated microtubules would lead to a further, detectable slow-down (Fig. 6). The initial speed of biotinylated gliding microtubules (Fig. 6, red bars) was decreased by 30% after streptavidin coating (Fig. 6, channel 1 and 2, green bars), while microtubules incubated with a control solution without streptavidin remained unaffected (Fig. 6, channel 3, green bar). Subsequent incubation with anti-SA-AB (100 nM, 10 min) decreased the speed significantly (p value $<< 0.01$) by another 70% (Fig. 6, channel 1, blue bar). The successful binding of anti-SA-AB to the microtubules was confirmed by fluorescence images taken in the FITC channel (data not shown). Control populations of biotinylated microtubules, that were (i) coated with streptavidin and incubated with a control solution without anti-SA-AB (Fig. 6, channel 2, blue bar) or (ii) not coated with streptavidin

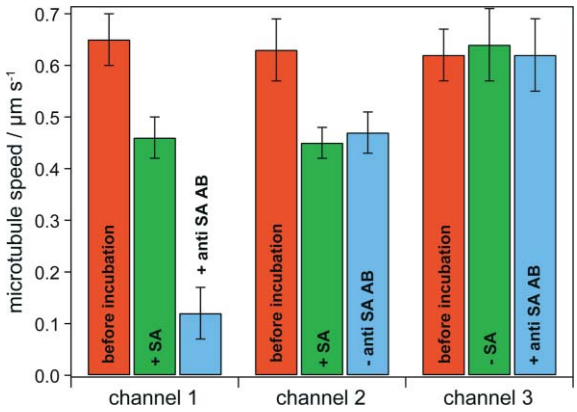

Fig. 6 Detecting anti-streptavidin antibodies (anti-SA-AB) using streptavidin-coated microtubules. Gliding speeds of microtubules in three independent flow channels. The speeds of representative microtubules were measured in each channel before treatment (red bars), after incubation with or without streptavidin (green bars) and after incubation with or without anti-SA-AB (blue bars). Error bars represent the standard deviations for 20 microtubules.

and incubated with anti-SA-AB (Fig. 6, channel 3, blue bar), remained unaffected. This shows that detection of an analyte which is linked to microtubules *via* a molecule that is comparable in size to a Fab fragment is possible. This additional slow-down indicates that the roadblock effect described above depends on the size of the obstacle. This seems unintuitive at first, since stopping at a roadblock should not depend on the size of the obstacle, once it is big enough to stop kinesin. However, kinesin's ability to overcome roadblocks (as observed in our data related to Fig. 3) might very well be dependent on the size of the obstacles. This size-dependent roadblock effect is interesting and will be the subject of further studies.

The detection limit of our proposed detection scheme can be estimated by the following considerations: For the case of streptavidin detection on biotinylated microtubules a significant ($p = 0.04$, Student's t-test) slow-down of about 5% (compared to the unbiotinylated control) is observed with presumably one streptavidin molecule bound to every hundredth tubulin dimer (lowest biotinylation ratio of 0.01 in Fig. 2B). Considering a microtubule geometry with 13 protofilaments and a dimer repetition length of 8 nm, this corresponds to a maximum of 16 streptavidin molecules per µm length of microtubule. Therefore, a total of about 600 molecules attached to 20 microtubules with an average length of 2 µm should suffice to detect significant speed differences. The detection sensitivity in terms of the lowest detectable concentration is determined by the dissociation constant of the linker and the analyte. Fab fragments and aptamers usually have dissociation constants in the range of nM which means that we can collect enough molecules for detection either (i) out of a very diluted large sample (limited by the dissociation constant of the Fab fragment or aptamer used for binding) or (ii) out of a relatively concentrated very small sample. Note, that the detection volume is only limited by the volume that microtubules can be immersed in experimentally. Therefore, it is conceivable to use the proposed method for the detection of proteins from single cells.

Highly sensitive label-free methods for the detection of proteins from solution based on carbon nanotubes[33,34]

microcantilevers[35] and surface plasmon resonance[36] have been described in the literature. However, the use of microtubules as detectors as described here has distinct advantages, which cannot be provided by other detection methods described so far. Our proposed molecular detection scheme can be extended to the sorting and concentrating of biomolecules in highly integrated devices. Different microtubule populations walking along elongated tracks could be separated either by their speed (due to different cargo densities and sizes) or by their fluorescence (possibly bar-coded) color. Such a separation of gliding microtubules based on their color can be achieved by steering microtubules gliding in microfabricated channels into respective reservoirs by an electric current[3,37] or hydrodynamic flow.[38] In these reservoirs, microtubules could be concentrated by an appropriate shape of the collector[39,40] for further analysis of the analyte.

Conclusions

By monitoring microtubule speeds in gliding assays, we characterized their slow-down as a function of streptavidin concentration on the microtubule lattice. In our stepping assays, we found that single kinesin molecules frequently stopped when they encountered streptavidin obstacles. We therefore attribute the slow-down of gliding microtubules to an obstruction of kinesin paths caused by streptavidin molecules acting as roadblocks, rather than to 'frictional' cargo–surface interactions. Beyond an improved understanding of motor interactions with cargo-laden microtubules— which can be used to optimize cargo density on microtubules without compromising gliding speeds— we demonstrated a novel molecular detection scheme. Being extendable to the detection of many other proteins, this method has the potential to be operated with extremely small sample volumes (down to the contents of single cells) and can be incorporated into highly-integrated, autonomously operating molecular sorting devices.

Acknowledgements

We thank R. Cross (Marie Curie Institute, Surrey, UK) for the plasmid of rkin430-GFP; C. Bräuer and D. Naumburger for technical support; F. Ruhnow for help with the tracking algorithms; Alf Månsson (University of Kalmar, Sweden) for fruitful discussions on the molecular detection scheme; Bert Nitzsche, Chris Gell, Cordula Reuther, Gero Fink, Leonid Ionov and Michael Berndt for helpful comments on the manuscript. This work was supported by the German Federal Ministry of Education and Research (Grant 03 N 8712), the Volkswagen Foundation, by the Gottlieb Daimler and Karl Benz Foundation and the Max-Planck-Society.

Notes and References

1 K. J. Bohm, J. Beeg, G. M. zu Horste, R. Stracke and E. Unger, *IEEE Trans. Adv. Packaging*, 2005, **28**, 571–576.
2 L. Ionov, M. Stamm and S. Diez, *Nano Lett.*, 2005, **5**, 1910–1914.
3 M. G. L. van den Heuvel, M. P. De Graaff and C. Dekker, *Science*, 2006, **312**, 910–914.
4 R. K. Doot, H. Hess and V. Vogel, *Soft Matter*, 2007, **3**, 349–356.
5 J. Howard, A. J. Hudspeth and R. D. Vale, *Nature*, 1989, **342**, 154–158.
6 M. Mazumdar, A. Mikami, M. A. Gee and R. B. Vallee, *Proc. Natl. Acad. Sci. U. S. A.*, 1996, **93**, 6552–6556.
7 S. J. Kron, Y. Y. Toyoshima, T. Q. P. Uyeda and J. A. Spudich, *Methods Enzymol.*, 1991, **196**, 399–416.
8 H. Hess, J. Clemmens, D. Qin, J. Howard and V. Vogel, *Nano Lett.*, 2001, **1**, 235–239.
9 A. Mansson, M. Sundberg, M. Balaz, R. Bunk, I. A. Nicholls, P. Omling, S. Tagerud and L. Montelius, *Biochem. Biophys. Res. Commun.*, 2004, **314**, 529–534.
10 M. Bachand, A. M. Trent, B. C. Bunker, G. D. Bachand and J. Nanosci, *Nanotechnology*, 2005, **5**, 718–722.
11 G. D. Bachand, S. B. Rivera, A. Carroll-Portillo, H. Hess and M. Bachand, *Small*, 2006, **2**, 381–385.
12 A. K. Boal, G. D. Bachand, S. B. Rivera and B. C. Bunker, *Nanotechnology*, 2006, **17**, 349–354.
13 S. Ramachandran, K. H. Ernst, G. D. Bachand, V. Vogel and H. Hess, *Small*, 2006, **2**, 330–334.
14 C. Brunner, C. Wahnes and V. Vogel, *Lab Chip*, 2007, **7**, 1263–1271.
15 D. L. Coy, M. Wagenbach and J. Howard, *J. Biol. Chem.*, 1999, **274**, 3667–3671.
16 K. R. Rogers, S. Weiss, I. Crevel, P. J. Brophy, M. Geeves and R. Cross, *EMBO J.*, 2001, **20**, 5101–5113.
17 A. Seitz and T. Surrey, *EMBO J.*, 2006, **25**, 267–277.
18 I. Crevel, M. Nyitrai, M. C. Alonso, S. Weiss, M. A. Geeves and R. A. Cross, *EMBO J.*, 2004, **23**, 23–32.
19 Y. Vugmeyster, E. Berliner and J. Gelles, *Biochemistry*, 1998, **37**, 747–757.
20 C. Leduc, F. Ruhnow, J. Howard and S. Diez, *Proc. Natl. Acad. Sci. U. S. A.*, 2007, **104**, 10847–10852.
21 C. L. Asbury, A. N. Fehr and S. M. Block, *Science*, 2003, **302**, 2130–2134.
22 A. Yildiz, M. Tomishige, R. D. Vale and P. R. Selvin, *Science*, 2004, **303**, 676–678.
23 S. Ray, E. Meyhofer, R. A. Milligan and J. Howard, *J. Cell Biol.*, 1993, **121**, 1083–1093.
24 W. O. Hancock and J. Howard, *Proc. Natl. Acad. Sci. U. S. A.*, 1999, **96**, 13147–13152.
25 C. L. Asbury, *Curr. Opin. Cell Biol.*, 2005, **17**, 89–97.
26 J. Helenius, G. Brouhard, Y. Kalaidzidis, S. Diez and J. Howard, *Nature*, 2006, **441**, 115–119.
27 B. H. Kwok, L. C. Kapitein, J. H. Kim, E. J. G. Peterman, C. F. Schmidt and T. M. Kapoor, *Nat. Chem. Biol.*, 2006, **2**, 480.
28 A. Seitz, H. Kojima, K. Oiwa, E. M. Mandelkow, Y. H. Song and E. Mandelkow, *EMBO J.*, 2002, **21**, 4896–4905.
29 R. Dixit, J. L. Ross, Y. E. Goldman and E. L. F. Holzbaur, *Science*, 2008, **319**, 1086–1089.
30 J. Peloquin, Y. Komarova and G. Borisy, *Nat. Methods*, 2005, **2**, 299–303.
31 M. Hirabayashi, S. Taira, S. Kobayashi, K. Konishi, K. Katoh, Y. Hiratsuka, M. Kodaka, T. Q. P. Uyeda, N. Yumoto and T. Kubo, *Biotechnol. Bioeng.*, 2006, **94**, 473–480.
32 R. Martinez-Neira, M. Kekic, D. Nicolau and C. G. dos Remedios, *Biosens. Bioelectron.*, 2005, **20**, 1428–1432.
33 R. J. Chen, S. Bangsaruntip, K. A. Drouvalakis, N. Wong, Shi Kam, M. Shim, Y. Li, W. Kim, P. J. Utz and H. Dai, *Proc. Natl. Acad. Sci. U. S. A.*, 2003, **100**, 4984–4989.
34 F. Patolsky, G. F. Zheng and C. M. Lieber, *Nat. Protocols*, 2006, **1**, 1711–1724.
35 G. H. Wu, R. H. Datar, K. M. Hansen, T. Thundat, R. J. Cote and A. Majumdar, *Nat. Biotechnol.*, 2001, **19**, 856–860.
36 C. Campagnolo, K. J. Meyers, T. Ryan, R. C. Atkinson, Y. T. Chen, M. J. Scanlan, G. Ritter, L. J. Old, C. A. Batt and J. Biochem, *Biophys. Methods*, 2004, **61**, 283–298.
37 L. L. Jia, S. G. Moorjani, T. N. Jackson and W. O. Hancock, *Biomed. Microdevices*, 2004, **6**, 67–74.
38 F. U. Gast, P. S. Dittrich, P. Schwille, M. Weigel, M. Mertig, J. Opitz, U. Queitsch, S. Diez, B. Lincoln, F. Wottawah, S. Schinkinger, J. Guck, J. Kas, J. Smolinski, K. Salchert, C. Werner, C. Duschl, M. S. Jager, K. Uhlig, P. Geggier and S. Howitz, *Microfluid. Nanofluid.*, 2006, **2**, 21–36.
39 Y. M. Huang, M. Uppalapati, W. O. Hancock and T. N. Jackson, *Biomed. Microdevices*, 2007, **9**, 175–184.
40 C. T. Lin, M. T. Kao, K. Kurabayashi and E. Meyhofer, *Nano Lett.*, 2008, **8**, 1041–1046.